

# Macroscopic Quantum Resonators (MAQRO)

**Lead Proposer:** Rainer Kaltenbaek

Proposal submitted by the MAQRO consortium consisting of following members in alphabetical order:

M. Arndt, University of Vienna, Austria	S. Hossenfelder, FIAS, Frankfurt, Germany
M. Aspelmeyer, University of Vienna, Austria	U. Johann, Airbus Defence & Space, Germany
P. Barker, University College London, UK	R. Kaltenbaek, University of Vienna, Austria
A. Bassi, University of Trieste, Italy	N. Kiesel, University of Vienna, Austria
J. Bateman, University of Swansea, UK	M. Kim, Imperial College London, UK
K. Bongs, University of Birmingham, UK	C. Lämmerzahl, ZARM, Univ. of Bremen, Germany
S. Bose, University College London, UK	G. J. Milburn, University of Queensland, Australia
C. Braxmaier, ZARM, University of Bremen, Germany	H. Müller, University of California, Berkley, USA
C. Brukner, University of Vienna, Austria	L. Novotny, ETH Zürich, Switzerland
B. Christophe, Onera, France	M. Paternostro, Queen's University Belfast, UK
M. Chwalla, Airbus Defence & Space, Germany	A. Peters, Humboldt University, Berlin, Germany
P.-F. Cohadon, LKB, France	A. Pilan Zanoni, CERN, Switzerland
C. Curceanu, INFN Frascati, Italy	E. M. Rasel, University of Hannover, Germany
L. Diósi, Wigner Research Inst. Phys, Hungary	C. J. Riedel, Perimeter Institute, Canada
K. Dholakia, University of St. Andrews, UK	M. Rodriguez, Onera, France
K. Döringshoff, Humboldt University, Germany	L. Rondin, ETH Zürich, Switzerland
W. Ertmer, University of Hannover, Germany	A. Roura, University of Ulm, Germany
A. Geraci, University of Nevada, Reno, USA	W. Schleich, University of Ulm, Germany
J. Gieseler, ETH Zürich, Switzerland	J. Schmiedmayer, TU Vienna, Austria
N. Gürlebeck, ZARM, Univ. of Bremen, Germany	T. Schuldt, DLR Bremen, Germany
G. Hechenblaikner, ESO, Germany	K. C. Schwab, Caltech, USA
A. Heidmann, LKB, France	M. Tajmar, TU Dresden, Germany
S. Herrmann, ZARM, University of Bremen, Germany	H. Ulbricht, University of Southampton, UK
	R. Ursin, IQOQI, Vienna, Austria
	V. Vedral, University of Oxford, UK

Proposal for **New Science Ideas in ESA's Science Programme**

## Contact Information

<b>Lead Proposer:</b>	Rainer Kaltenbaek
<b>Address</b>	<b>Contact</b>
Vienna Center for Quantum Science & Technology Faculty of Physics University of Vienna Boltzmannngasse 5 1090 Vienna Austria	<i>Mobile:</i> +43 664 1561372 <i>Tel:</i> +43 1 4277 72534 <i>Fax:</i> +43 1 4277 8 72534 <i>e-mail:</i> rainer.kaltenbaek@univie.ac.at

*The Lead Proposer hereby confirms his availability for supporting the study activities throughout the study period.*

A handwritten signature in black ink, appearing to read 'R. Kaltenbaek', with a long horizontal stroke extending to the right.

**Rainer Kaltenbaek**

## 1. Executive summary

The last decade has witnessed impressive progress in space and quantum technology. LISA Pathfinder created new benchmarks for optical technology and microgravity available in space and paved the road towards the future observation of gravitational waves in space [1]. On ground, the efforts to devise interferometric techniques to observe gravitational waves finally succeeded [2]. This was the driving force behind developing measurement techniques at the quantum limit [3,4], which led to cooling mechanical resonators to the quantum regime [5–7].

MAQRO represents the unique endeavor to combine this progress in space and quantum technologies by taking full advantage of novel space technology to test the foundations of quantum in deep space. Quantum physics challenges our understanding of physical reality and space-time. Testing quantum phenomena like quantum superpositions involving macroscopic objects provides novel insights into such fundamental questions: do the laws of quantum physics still hold for macroscopic objects or do yet unknown effects set a limit for massive objects? What is the fundamental relation between quantum physics and gravity?

The **main scientific objective** of MAQRO is to test quantum theory in a hitherto inaccessible regime of quantum superpositions of macroscopic objects containing up to  $10^9$  atoms. This is achieved using techniques from quantum optomechanics, matter-wave interferometry and optical trapping. MAQRO will test quantum physics for parameters 6 orders of magnitude beyond existing experimental tests. This promises decisive tests of theoretical models predicting deviations from quantum physics [8–10]. By pushing the limits of state-of-the-art experiments and by taking advantage of deep space for macroscopic quantum experiments, MAQRO may prove a **pathfinder for quantum technology in space** – e.g., for using quantum optomechanics in high-sensitivity measurements like future gravitational-wave observatories.

The **case for space** is to overcome or push the limits of ground-based tests like limited free-fall time, vibrations, and environmental decoherence. The latter results, e.g., from interactions with gas or blackbody radiation. The spacecraft design of MAQRO overcomes these limitations by offering a unique environment of micro-gravity ( $\lesssim 10^{-9}$  g), low pressure ( $\lesssim 10^{-13}$  Pa) and low temperature ( $\lesssim 20$  K). This sufficiently suppresses quantum decoherence to allow performing macroscopic quantum experiments with free-fall times of about 100 s.

MAQRO benefits from significant **technological heritage** in space technology. In particular, it relies on heritage from LISA Pathfinder (LPF), the LISA technology package (LTP), GAIA and the James Webb Space Telescope (JWST). The spacecraft, launcher, ground segment and orbit (L1/L2) are as in LPF. Modifications to the LPF design are an external, passively cooled optical instrument thermally shielded from the spacecraft, and the use of two capacitive inertial sensors.

In 2010 and 2015, MAQRO was proposed as a medium-sized mission to the European Space Agency (ESA) in response to ESA’s Cosmic Vision calls for medium-size mission opportunities “M3” and “M4”, respectively. While significant progress has been achieved since the original proposal, and while the science case of MAQRO has been received very positively, some technological aspects of the proposal were deemed to be of too low technological readiness level (TRL). With the present proposal in response to ESA’s call for “New Science Ideas”, we want to enter a more detailed discussion with ESA to improve the MAQRO mission proposal and to refine the roadmap for technology development to increase the overall TRL in preparation for future mission calls.

## 2. Science Case

Schrödinger’s famous thought experiment of a dead-and-alive cat [11] addresses a crucial question of quantum physics: do the laws of quantum physics remain applicable without modification up to the macroscopic level? Matter-wave experiments have confirmed the quantum physics from the level of electrons [12,13], atoms and small molecules [14] up to massive molecules with  $10^4$  atomic mass units (amu) [15]. Still, such experiments are far from a mass regime where alternative theories predict deviations from quantum physics [10,16].

Using increasingly massive test particles on Earth may soon face principal limitations due to limited free-fall times and the limited quality of vibration isolation and microgravity. This limit may be reached already with test masses between  $10^6$  and  $10^8$  amu [17]. While a recent proposal suggests using magnetically levitated microspheres for ground-based tests of quantum physics with higher test masses [18], potential technological limitations have not yet been studied in sufficient detail to decide whether this approach may indeed overcome the limitations faced by more established techniques. With MAQRO, we propose to address these challenges by harnessing a deep-space environment for experiments using high-mass matter-wave interferometry [19,20] and quantum optomechanics for quantum-state preparation and high-sensitivity measurements [21]. MAQRO aims to significantly advance present limits of high-mass matter-wave interferometry to test quantum physics with particle masses up to  $\sim 10^{10}$  amu. Our proposal not only promises high-precision tests of the foundations of quantum physics and decisive tests of alternative theories known as “collapse models”, which predict notable deviations from the predictions of quantum theory. By increasing the technological readiness of quantum optomechanics in space our proposal would also benefit future applications in high-sensitivity measurements like gravitational-wave detection (see, e.g., [22,23]).

An important feature of MAQRO is that the parameter range covered has some overlap with experiments that should be achievable on ground. This allows cross-checking the performance of MAQRO and provides a fail-safe in case the predictions of quantum physics should fail already for masses less than  $10^8$  amu. Even in the presence of strong non-quantum decoherence mechanism that would prevent MAQRO from observing matter-wave interference, using alternative experimental operation modes, MAQRO could still characterize the evolution of macroscopic quantum states in an environment unlike any achievable on Earth. For this reason, the MAQRO instrument allows multiple scientific modes as indicated below:

- **Heating of the center-of-mass motion**  
This a novel idea is based on a recent proposal using hybrid optical and a Paul traps [24]. Due to its novelty, it would have to be analyzed more closely in a study phase resulting from this proposal. The goal is to observe heating of the motion of a trapped particle due to decoherence mechanisms. While this method does not require freely falling test, it would still benefit from the low-decoherence environment of MAQRO.
- **Wave-packet expansion**  
As in the approach on heating of the center-of-mass motion, this method is based on the stochastic momentum transfer due to collapse mechanisms. In particular, the momentum transfer leads to a random walk resulting in an increased rate for the expansion of wave packets [25–27]. This can be studied by monitoring the time evolution of freely falling test particles.
- **High-mass matter-wave interferometry**  
This is the central experiment of MAQRO. Since the original M3 proposal [19], this experiment has been updated in the course of the M4 proposal to harness Talbot-Lau

matter-wave interferometry [20], which currently holds the mass record for matter-wave interferometry [15]. The goal is to observe matter-wave interferometry with particles of varying size and mass, comparing the interference visibility to the predictions of quantum theory and to the predictions of alternative theoretical models.

In addition to promising interesting scientific results in their own right, the first two techniques can be used for calibrating the instrument and as fallback options if strong decoherence should prevent observing high-mass matter-wave interference. If these two tests show agreement with the predictions of quantum physics, MAQRO's scientific instrument can then be used for performing matter-wave interferometry to test for smaller deviations from quantum physics.

MAQRO will test for deviations from the predictions of quantum physics by performing high-precision measurements in the context of the free evolution of quantum wave packets and in the context of macroscopic quantum superpositions. Such deviations can be described as modifications to the von Neumann equation [28]:

$$\frac{d\hat{\rho}}{dt} = -\frac{i}{\hbar} [\hat{H}, \hat{\rho}] + \Lambda [\hat{x}, [\hat{x}, \hat{\rho}]]. \quad (1)$$

This equation describes the time evolution of a density operator  $\hat{\rho}$ , which describes the state of a quantum system. Here,  $\hat{H}$  is the Hamiltonian of the system,  $\hat{x}$  is the position operator,  $\hbar$  is Planck's constant, the square brackets denote the commutator  $[a, b] = ab - ba$ , and  $\Lambda$  is a parameter describing potential deviations from quantum evolution. For  $\Lambda = 0$ , we recover the standard von Neumann equation of quantum physics. Density operators are a generalization of pure quantum states, which evolve according to Schrödinger's equation.

The above equation holds for weak, possibly unknown interactions with the quantum system. Known interactions like the scattering of gas molecules or blackbody radiation can also be described in this way. Such interactions lead to decoherence of the quantum system, i.e., increasingly "classical" behavior. By "classical" we refer to behavior according to the laws of classical physics (Newton, Maxwell, and Einstein), i.e., the absence of quantum effects like superposition, interference or entanglement. Since decoherence effects are additive, we can, e.g., use the sum  $\Lambda = \Lambda_{\text{QM}} + \Lambda_{\text{CM}}$  to describe the overall decoherence according to quantum physics ( $\Lambda_{\text{QM}}$ ) plus additional decoherence  $\Lambda_{\text{CM}}$  due to alternative "collapse models" [10].

The central goal of MAQRO can therefore be described as experimentally determining  $\Lambda$  as precisely as possible and to test whether it deviates from the value  $\Lambda_{\text{QM}}$  predicted by quantum physics. This is achieved in the following way using the three experimental modes available:

- **Heating of the center-of-mass motion**  
Any  $\delta\Lambda$  leading to deviations  $\Lambda = \Lambda_{\text{QM}} + \delta\Lambda > \Lambda_{\text{QM}}$  from the predictions of quantum physics will result in a more rapid increase in the mean occupation number of the quantum harmonic oscillator describing the motion of a trapped test particle.
- **Wave-packet expansion**  
Here, one tests for deviations from the predictions of quantum physics by releasing a test particle from its trap and observing its free evolution. Once the particle is released, the wave packet describing the quantum state of the particle will expand more rapidly than predicted by quantum physics if  $\Lambda > \Lambda_{\text{QM}}$ .
- **High-mass matter-wave interferometry**  
When we observe matter-wave interference, any deviations from the predictions of

quantum physics can lead to a reduction of the interference visibility. By varying experimental parameters like particle size and material, one could study the parameter dependence of such deviations.

The predictions of existing alternative theoretical models like “collapse models” [10] can provide benchmarks indicating parameter regions for tests of quantum physics. Such models typically predict values or ranges of  $\Lambda_{\text{CM}}$  we can use to analyze which deviations MAQRO would be sensitive to. In Figure 1, we plot the predictions of various collapse models and compare them with the minimum deviations  $\Lambda$  MAQRO could detect using the three experimental approaches described above. High-mass matter-wave interferometry would allow testing for significantly smaller deviations  $\Lambda_{\text{CM}}$  than the experiment monitoring wave-packet expansion, and this again would be more sensitive than measuring heating of the center-of-mass motion.

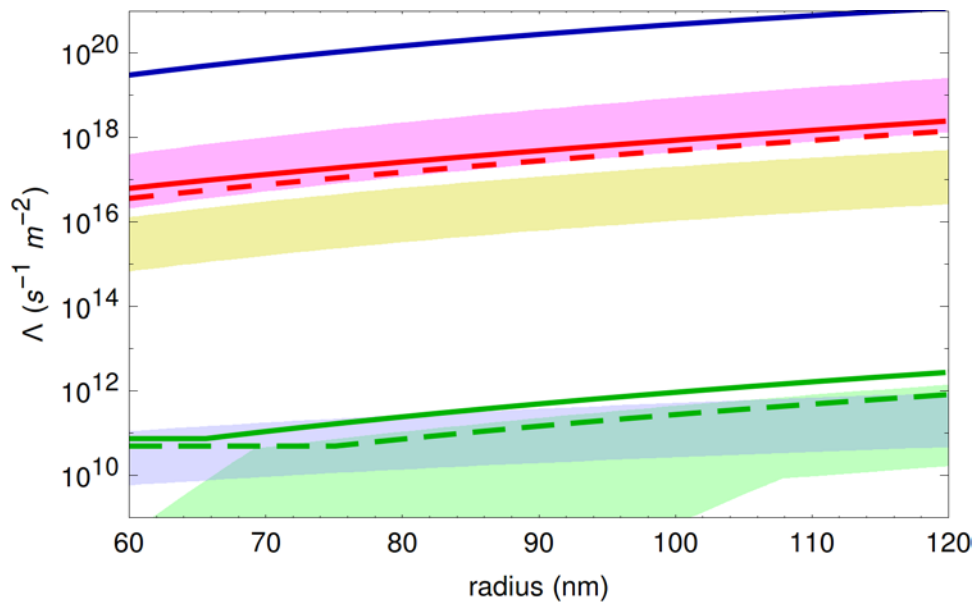


**Figure 1: Theoretical predictions and experimental sensitivity vs test-particle radius.** The shaded regions indicate the predictions of the decoherence parameter  $\Lambda$  for the mass density of the test particle varying between  $2200 \text{ kg m}^{-3}$  (fused silica) and  $9680 \text{ kg m}^{-3}$  (Hafnia). Green: K model, Blue: DP model, Yellow: CSL model, Magenta shaded: QG model. Green, solid line: minimum  $\Lambda$  discernible using high-mass matter-wave interferometry. Red, solid line: minimum  $\Lambda$  discernible using wave packet expansion. Blue, solid line: minimum  $\Lambda$  discernible observing heating of the motion in a hybrid trap. The dashed lines shows the potential for improvement by allowing for longer free-fall times. We will describe how we arrive at these predictions in section 3.

In the following, we will provide a short overview of the collapse models used in Figure 1 to benchmark the potential performance of the MAQRO instrument:

- **Continuous Spontaneous Localization (CSL model)**

The CSL model is a heuristic model originally devised to describe a continuous transition from quantum to classical behavior as the size and mass of a physical system increases [29–32]. The physical interpretation is that any constituent of matter is subject to decoherence with a rate  $\lambda_{\text{CSL}}$  and a typical length scale  $r_c$ . While  $r_c$  is consistently assumed to be on the order of 100 nm, values for  $\lambda_{\text{CSL}}$  range from  $2.2 \times 10^{-17} \text{ Hz}$  to  $10^{-8 \pm 2} \text{ Hz}$  [33]. In Figure 1, we assumed  $2.2 \times 10^{-17} \text{ Hz}$ .

- **Quantum Gravity (QG model)**

Ellis and co-workers suggested [34] that future models of quantum gravity may lead to

the decoherence of macroscopic quantum superpositions.

- **Diósi-Penrose (DP model)**  
 Diósi assumes non-linear Schrödinger-Newton type deviations from quantum physics where one assumes the wave function to describe a mass density exhibiting self-gravitation [35]. This leads to decoherence for macroscopic quantum superpositions. Using a completely different approach, Penrose arrives at similar predictions arguing that macroscopic superpositions lead to a decaying superposition of different space-time curvatures [36].
- **Károlyházy (K model)**  
 Károlyházy devised one of the first collapse models [37]. He predicts decoherence of macroscopic superpositions due to quantum fluctuations of the underlying space-time.

Figure 1 shows that MAQRO has the potential to perform decisive tests of all these models. At the same time, even if none of these models should be valid, MAQRO would allow to significantly extend the parameter range over which quantum physics has been tested, to study the parameter dependence of known decoherence mechanisms and to potentially uncover deviations from the predictions of quantum physics not covered by any of the models above.

### 3. Scientific requirements

Here, we will first outline the measurements to be performed to achieve the scientific objectives. We will use these descriptions to explain the resulting scientific requirements. Finally, we will define a baseline configuration and present a summary of the scientific requirements.

#### 3.1. Heating of the center-of-mass motion

In the CSL model, each constituent particle of a quantum system is localized at a decoherence rate  $\lambda_{\text{CSL}}$  due to the interaction with a fluctuating, classical field [25]. This interaction imparts momentum kicks to the quantum system. In two recent proposals, it was suggested to observe the effect of this mechanism on mechanical oscillators [24,38]. In particular, in the case of a trapped test particle described as a quantum harmonic oscillator, the momentum kicks will result in an additional heating mechanism in the motion of the harmonic oscillator and an increase in the mean occupation number of the oscillator over time [24].

In order to observe this heating effect, any competing heating effects, e.g., due to collisions with gas molecules or due to the scattering, absorption and emission of blackbody radiation has to be kept small in comparison. Because the heating due scattering of photons would be much stronger than the heating due to the CSL mechanism, one cannot use an optically trapped particle to observe this effect. For this reason, it was suggested to use a hybrid trap instead, where an optical field is used to cool the center-of-mass motion of a charged particle in a Paul trap [24,39]. To observe the heating due to the CSL mechanism, the optical field has to be switched off. In Ref. [24], the mechanical frequency in the Paul trap was assumed to be 5 kHz for a fused-silica particle with a radius of 100 nm.

In earlier proposals of MAQRO, we have assumed purely optical trapping of the test particle during the experiments. Only in transporting the test particles to the trap did we consider also using Paul traps [20]. To test for heating of the center-of-mass motion as described above, we

would also need to include a Paul trap on the optical bench itself. Since this will require a modification of the scientific instrument, we include this measurement as an **optional extension** of the MAQRO proposal. It will require further study to adapt the proposed instrument accordingly. A possible solution is to include a surface-electrode point Paul trap [40] on the optical bench, which would be compatible with MAQRO's approach of passive radiative cooling [41].

### 3.2. Wave-packet expansion

The same mechanism of momentum diffusion heating the center-of-mass motion of a trapped test particle as described in section 2.1 also leads to a quicker expansion of the wave packet of a free particle. This effect was first described by Collett and Pearle [25] and later analyzed in the context of MAQRO [26], and the feasibility of testing this effect in the laboratory using state-of-the-art technology was investigated in Ref. [27].

The width of a wave packet  $w(t)$  as a function of time  $t$  is:

$$w(t)^2 = \langle \hat{x}^2(0) \rangle + \frac{t^2}{m^2} \langle \hat{p}^2(0) \rangle + \frac{2\Lambda \hbar^2}{3m^2} t^3. \quad (2)$$

$m$  is the mass of the particle,  $\hat{x}$  and  $\hat{p}$  denote the position and momentum operators, respectively, and angular brackets denote the expectation value for a given quantum state. We see that the wave packet will expand over time even in the absence of decoherence ( $\Lambda = 0$ ) due to momentum uncertainty. In this case, we denote the width of the wavepacket as  $w_s$ . For  $\Lambda > 0$ , the width of the wave packet increases more quickly.

That means, we can determine the strength of decoherence acting on a freely evolving particle by observing the time evolution of the width of the wave packet. This width is not an observable and has to be determined from the statistical distribution in repeated measurements [42]. If we perform  $N$  measurements of the particle position, and if the result of the  $j$ -th measurement is  $x_j$ , then the width of the wave packet is given by:

$$w = \lim_{N \rightarrow \infty} \frac{1}{\sqrt{N-1}} \left( \sum_{j=1}^N x_j^2 \right)^{1/2}. \quad (3)$$

The fractional uncertainty of the width of the wave packet will be:

$$\frac{\Delta w}{w} = [2(N-1)]^{1/2}. \quad (4)$$

If the additional expansion of the wave packet is small, we can then approximate  $\Delta w \simeq w_s [2(N-1)]^{-1/2}$ . To determine the decoherence parameter  $\Lambda$  using equation (2), one has to measure the width of the wavepacket at multiple times  $t$  in order to estimate the contributions of the constant term as well as the terms quadratic and cubic in time  $t$ . Given a known initial quantum state at  $t = 0$ , it is sufficient to measure the width of the wave packet at one later time  $t = T > 0$ . Ideally,  $T$  should be as large as possible to clearly see the additional spreading due to decoherence. There are, however, two limitations to  $T$ : (1), if  $T$  is too long, the spread of the wave packet will become larger than the optically accessible region for measuring the particle position via optical scattering. (2), the mission life time will, of course, be limited. The first restriction limits the time  $T$  to about 100 s. Then the second restriction will require a measurement series to take at most a time on the order of one month. This results in at most  $\lesssim 3 \times 10^4$  data points.

To experimentally determine  $\Lambda$ , the additional increase in the width of the wave packet has to be larger than the statistical uncertainty of the measured width of the wave packet. That means, we must have:

$$\Lambda > \Lambda_{\min} = 3 m^2 \frac{w_s^2(t)}{\sqrt{2(N-1)} \hbar^2 T^3}. \quad (5)$$

Moreover, to best see potential deviations from the predictions of quantum physics:  $\Lambda_{\min} \gg \Lambda_{\text{QM}}$ . This condition allows us to define scientific requirements for this experiment. To this end, we have to carefully analyze the decoherence effects determining  $\Lambda_{\text{QM}}$ .

We now need to discuss the limitations on the original quantum state. Because the wave packet will expand freely for a very long time, we need to ensure that the size of the wave packet remains small enough such that we can measure the position of the particle via optical scattering. We restrict ourselves to optical modes with a waist of at most 1 mm and therefore have to place an upper limit on  $w(T)$ . A realistic upper limit is 0.3 mm. We can fulfill this condition if we achieve an initial thermal occupation of  $n = 0.3$  for a mechanical frequency of  $\omega = 10^5$ .

The solid red line in Figure 1 shows of  $\Lambda_{\min}$  for the baseline parameters given in subsection 3.4. For the dashed, red line in the same figure, we used an increased free-fall time of  $T = 150$  s to illustrate the potential for improving the testable parameter range. While the improvement is not large, in this case, one could test CSL with decoherence rates as low as  $2.2 \times 10^{-17}$  Hz even with the small mass density of fused silica.

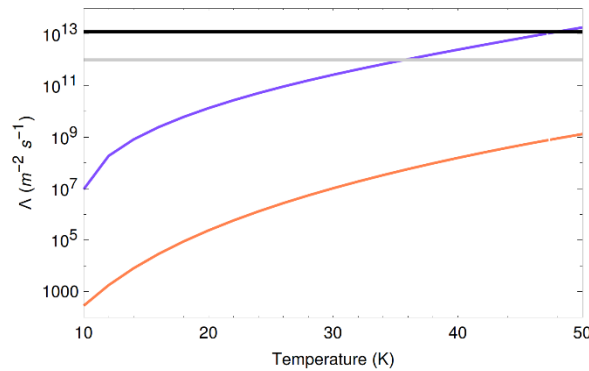


**Figure 2: Decoherence due to blackbody radiation.** Red, solid line: scattering of blackbody radiation. Blue, solid line: absorption (emission) of blackbody radiation as a function of environment (test particle) temperature. Black, solid line:  $\Lambda_{\min}$ . Gray, solid line:  $\Lambda_{\min}/10$ .

For an uncharged test particle in free fall, the main decoherence mechanisms are the scattering of gas molecules and the scattering, absorption and emission of blackbody radiation. In Figure 2, we compare decoherence rates due to blackbody radiation for a fused-silica test particle with 100 nm radius with  $\Lambda_{\min}$  calculated for  $T = 100$  s and a 30-days measurement series. The plot shows that our condition  $\Lambda_{\min} \gg \Lambda_{\text{QM}}$  is fulfilled for temperatures below 35 K.

Given this limit on the environment temperature, we can now analyze the requirements due to decoherence resulting from gas collisions. The wavelength of the gas molecules at 35 K will be on the order of  $10^{-2}$  nm. This is much smaller than the radii of the test particles used and, already after a very short time, that wavelength will be much smaller than the extension of the wave packet. For that reason, collisions with gas molecules can be treated in the short-wavelength limit, and the corresponding decoherence rate is [28,43]:

$$\gamma_{\text{gas}} = 16 \sqrt{2\pi/3} P r^2 / (m_g v_g), \quad (6)$$

Where  $m_g$  and  $v_g$  are the mass and the velocity of the gas molecules, respectively,  $P$  is the pressure, and  $r$  is the radius of the test particle. Because already a single collision can decohere the wave packet the decoherence rate must fulfill  $\gamma_{\text{gas}} \ll T^{-1}$  to ensure coherent evolution during the time of wave-packet expansion. For a test particle with  $r = 100$  nm and  $T = 100$  s, we therefore require  $P \lesssim 10^{-13}$  Pa. If this condition is fulfilled, we can neglect decoherence due to gas collisions.

Because stray electromagnetic fields and nearby charges on the scientific instrument could significantly influence the free evolution of the test particle if it was charged, we require the test particle to have zero charges.

Apart from these requirements on the particle and environment properties, it is paramount that our accuracy  $\sigma$  in determining the position of the test particle is better than  $\Delta w$ . For a fused-silica particle with  $r = 100$  nm, a measurement time  $T = 100$  s, 30 days of measurements, a mechanical frequency of  $\omega_m = 10^5$  rad/s, and an initial occupation of 0.3, this results in the requirement  $\sigma \ll \Delta w \cong 420$  nm.

### 3.3. High-mass matter-wave interferometry

As can be seen in Figure 1, using matter-wave interferometry with high-mass test particles is the most sensitive tool of MAQRO for testing quantum physics. The original MAQRO proposal for ESA's "M3" call proposed to perform far-field, double-slit-type matter-wave interference. For the "M4" proposal of MAQRO, we adapted near-field matter-wave interferometry [20] instead. Advantages of this technique are that it is well established in state-of-the-art experiments [44], that it allows high-visibility interference, and that the technologies required are more mature.

This approach is based on a recent proposal for ground-based high-mass matter-wave interferometry [17]. First, a test particle is optically trapped and cooled using optomechanical techniques [21]. Then the particle is released and evolves in free fall for some time  $t_1$ . Then an optical field (wavelength  $\lambda_g$ ) is switched on for a short time  $\tau$ , creating a standing-wave phase grating with a period  $d = \lambda_{sw}/2$ , applying the position-dependent phase  $\phi(x) = \phi_0 \cos^2(2\pi x/\lambda_{sw})$  to the quantum state. After that, the particle will evolve again for a time  $t_2$ , and then we measure the position of the particle, and repeat the whole process  $N$  times. Due to the limitations we discussed in section 3.2, the times of free fall should fulfill  $T = t_1 + t_2 \lesssim 100$  s.

Once we have collected sufficient data, we can study the histogram of the recorded positions. If the quantum state before the application of the phase grating covers a sufficiently high number of nodes of the grating, and if  $t_2/\mu$  is an integer multiple of the Talbot time  $t_T = \frac{md^2}{h}$  with  $\mu = T/t_1$ , quantum physics predicts that the histogram of recorded positions will show an interference pattern with a period  $\mu d$  [17,20]. Here, we used Planck's constant  $h$  and the mass  $m$  of the test particle. Due to a moiré shadowing effect, one can also observe an interference-like pattern for purely classical particles [45]. As can be seen in the example provided in Figure 3, for a proper choice of experimental parameters, this classical pattern will, however, be very different from the pattern according to quantum physics.

In order to derive the scientific requirements, let us consider the interference pattern predicted

by quantum theory:

$$P(x) = \frac{m}{\sqrt{2\pi}\sigma_p T} \sum_{n=-\infty}^{\infty} \exp[i n k_g x] J_{2n}[\phi_0 \sin(\pi n \kappa)] \exp\left[-\frac{1}{2}\left(2\pi n \frac{t_2}{T} \frac{\sigma_x}{d}\right)^2\right] \exp\left[-\frac{\Lambda T (n\kappa d)^2}{3}\right]. \quad (7)$$

Here, we have introduced several new definitions:  $k_g = 2\pi/\mu d$ ,  $\alpha = t_1/t_T$ ,  $\beta = t_2/t_T$ ,  $\kappa = \alpha\beta/(\alpha + \beta)$ , and  $J_n(x)$  is a Bessel function of the first kind.  $\sigma_x$  and  $\sigma_p$  are parameters describing the initially prepared quantum state. Its characteristic function is [20]:

$$\chi_0(s, q) = \exp\left(-\frac{\sigma_x^2 q^2 + \sigma_p^2 s^2}{2 \hbar^2}\right). \quad (8)$$

In equation (7), there are two exponential factors that potentially reduce the interference visibility. The one depending on  $\Lambda$  is, of course, due to decoherence. The other one depends on the initial quantum state, the grating period and the times  $t_{1,2}$  chosen. In order to achieve reasonable visibility despite the latter exponential factor, we must have  $\sigma_x/d \ll 1$ . That means, the original state should be nearly point like. Moreover, the visibility will depend on the Bessel function. One has to choose  $\phi_0$  appropriately to get maximum visibility. The prediction for the classical interference-like pattern can be calculated by replacing  $\sin(\pi n \kappa)$  with  $\pi n \kappa$  in equation (7). One can show that  $\kappa$  must fulfill  $\kappa \leq T/(4 t_T)$ . However, to make the quantum prediction clearly distinct from the classical prediction,  $\kappa$  should not be chosen too small. That means,  $T$  should not be much smaller than  $t_T$ . The shorter the wavelength for the phase grating, the easier it is to fulfill this condition even for large test masses. However, due to the transparency of the test particles and the laser technology in space, the shortest realistic wavelength possible is  $\lambda_g \cong 200$  nm. For a maximum free-fall time of  $T = 100$  s, this sets an upper limit of  $10^{10}$  amu for the mass of the test particles.

Now, let us estimate requirements on the original quantum state. If we assume that it is a thermal state of a harmonic oscillator, we have  $\sigma_x = [\hbar (1 + 2n)/(2m\omega)]^{1/2}$ . Requiring  $\sigma_x/d < 10^{-1}$ , we get an upper limit on the occupation number  $n \lesssim n_{\max} = 10^{-2} m \omega \frac{d^2}{\hbar} - \frac{1}{2}$ . We can now derive a requirement on  $\omega$ . In order to resolve the interference pattern, we need about 10 data points per interference fringe. The spacing of the fringes is  $\mu d$ , and the width of the measured particle positions can be approximated as  $w(T)$ . From these considerations, we get an upper limit  $\omega \lesssim \omega_{\max} = N_0/(T \sqrt{\eta})$ , where  $\eta = n/n_{\max}$  and  $N_0$  is the total number of data points recorded. For an appropriate choice of parameters ( $T = 100$  s,  $\eta = 0.1$ ,  $N_0 \cong 26 \times 10^3$ ), we find  $\omega_{\max} = 800$  rad/s. This results in  $n \cong 700$ ,  $\sigma_x/d = 0.03$ , and  $\sigma_p d/\hbar \cong 3500$  for a fused-silica particle with a radius of 100 nm. In Figure 3, we plot the corresponding quantum and classical predictions of the interference pattern (for  $\kappa \cong 0.94$ ,  $\alpha \cong 1.5$ ,  $\beta \cong 2.5$ , and  $m = 10^9$  amu).

Given that the period of the interference pattern is in the order of 200 nm, the accuracy of our position measurements should be  $\leq 20$  nm so we can resolve the interference pattern.

For masses up to  $10^9$  amu, we should be able to observe high-visibility Talbot-type interference. For masses beyond that, the limit  $\kappa \leq T/(4 t_T)$  will result in the quantum and classical predictions to become more and more similar for increasing masses because  $\sin(\pi n \kappa) \cong \pi n \kappa$  for small  $\kappa$ .

In the presence of decoherence, the interference visibility drops as plotted in Figure 4. The plot was calculated for a mass  $m = 10^9$  amu,  $T = 100$  s and  $d = 100$  nm. For smaller masses, we may, in principle, even choose shorter times  $T < 100$  s. However, the phase  $\phi_0$  experienced by

our particles for a given power of standing-wave phase grating will decrease with decreasing particle size. Every decrease in mass therefore has to be compensated by higher intensity in the phase grating in order to achieve the same phase shift. For the smallest particles used in MAQRO, one therefore may have to switch to longer wavelengths for the phase grating.

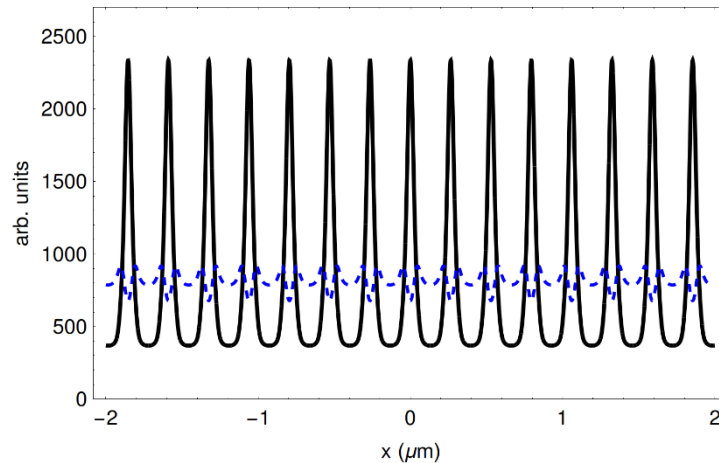


**Figure 3: Interference patterns.** Example of comparing the interference pattern predicted by quantum physics (black, solid line) and the interference-like pattern according to classical physics (blue, dashed line).

Figure 4 shows that we will not see any change to the interference visibility if  $\Lambda$  is too small, and we will not see any interference if  $\Lambda$  is too large. By requiring that the reduction factor plotted in Figure 5 is within a range  $[0.01, 0.99]$ , we can therefore define a range  $[\Lambda_{\min}, \Lambda_{\max}]$  our experiment will be sensitive to. The green solid and dashed lines in Figure 1, represent  $\Lambda_{\min}$  for free-fall times of 100s and 150s, respectively.

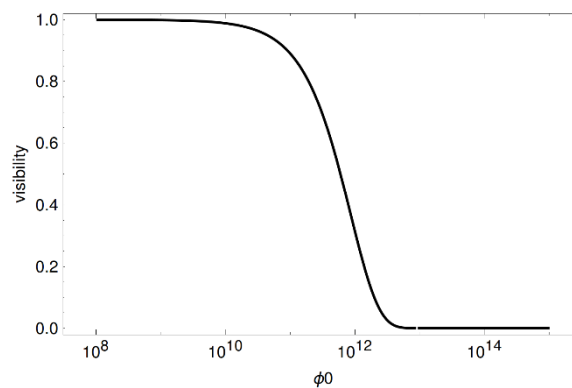


**Figure 4: Visibility reduction due to decoherence.** Quantum interference visibility reduces as a function of the strength of decoherence, parameterized by the parameter  $\Lambda$ .

We already saw in section 3.2 that pressure of the residual gas has to fulfill  $P \lesssim 10^{-13}$  Pa. The same holds true in the case of testing quantum physics using high-mass matter-wave interferometry. The requirements on the temperatures of the test particles and the environment are, however, more strict. In particular, we need the decoherence due to the scattering, emission and absorption of blackbody radiation to fulfill  $\Lambda \ll \Lambda_{\min}$ . From Figure 1, we can conclude that we need to fulfill  $\Lambda \ll 10^{-11} \text{ m}^{-2}\text{s}^{-1}$ , and from Figure 2, we conclude that the temperatures of the environment and the test particle should be below 25 K. Given that the particle temperature will always be higher than the environment temperature, we conservatively put the upper limit of  $T < 20$  K on the environment temperature.

### 3.4. Overview of the scientific requirements and baseline parameters

In the following, we define the baseline scientific requirements and parameters for MAQRO. As we discussed in section 3.1, we will need to study potential experiments on the heating of the motion of a trapped particle more thoroughly to provide the specific scientific requirements. However, these should be even more relaxed than in the case of experiments on the expansion of wave packets because the experiment does not require long free-fall times. Apart from requiring that the test particles are charged and trapped in a Paul trap, the requirements should be the same as for observing the expansion wave packets.

Parameter	Requirement
Nominal mission lifetime (without possible extension)	2 years
Environment temperature	< 35K
Residual-gas pressure	$\lesssim 10^{-13}$ Pa
Accuracy of position measurements	$\lesssim 500$ nm
Occupation number of initial thermal state	$\lesssim 1$
Mechanical frequency for initial preparation	$\cong 10^5$ rad/s
Test particles	
Mass	$10^8$ amu - $10^{10}$ amu
Charge	$0 e^-$
Type	dielectric, transparent at 1064nm
Size	30nm – 120nm
Temperature	$\lesssim 35$ K
Measurement time per data point	$\lesssim 100$ s

Table 1: Overview of the baseline scientific requirements for observing wave-packet expansion.

Consequently, we will only provide the scientific requirements for experiments on wave-packet expansion and on matter-wave interference based on the discussions in sections 3.2 and 3.3, respectively. These parameters are presented in Table 1 and Table 2. The requirements for high-mass matter-wave interferometry are the strictest. That means, if MAQRO fulfills the scientific requirements for high-mass matter-wave interferometry, it will also fulfill the requirements for the other two experimental modes. The only difference is in the requirements on the initial quantum state.

We assume a nominal lifetime of two years as the base line configuration because a shorter mission lifetime would significantly impede the number of experimental runs that could be performed, given that a full set of measurements can take one month or even longer. In particular, this would be the case if one also wants to perform runs with slightly longer free-fall times (e.g., 150s instead of 100s as illustrated in Figure 1).

Figure 5 is based on the scientific requirements provided in Table 1 and Table 2. In particular, the gray-shade region indicates the values of  $\Lambda$  as a function of particle radius that are not accessible to be tested using MAQRO because in that region decoherence predicted by quantum theory due to interactions with blackbody radiation would mask any potential deviations from the predictions of quantum physics.

Parameter	Requirement
Nominal mission lifetime (without possible extension)	2 years
Environment temperature	$< 20\text{K}$
Residual-gas pressure	$\lesssim 10^{-13}\text{ Pa}$
Accuracy of position measurements	$\ll 100\text{ nm}$
Occupation number of initial thermal state	$\lesssim 700$
Mechanical frequency for initial preparation	$\lesssim 800\text{ rad/s}$
Test particles	
Mass	$10^8\text{ amu} - 10^{10}\text{ amu}$
Charge	$0\text{ e}^-$
Type	dielectric, transparent at $1064\text{nm}$
Size	$30\text{nm} - 120\text{nm}$
Temperature	$\lesssim 25\text{ K}$
Period of phase grating	$100\text{nm}$
Measurement time per data point	$\lesssim 100\text{s}$

Table 2: Overview of the baseline scientific requirements for high-mass matter-wave interferometry.

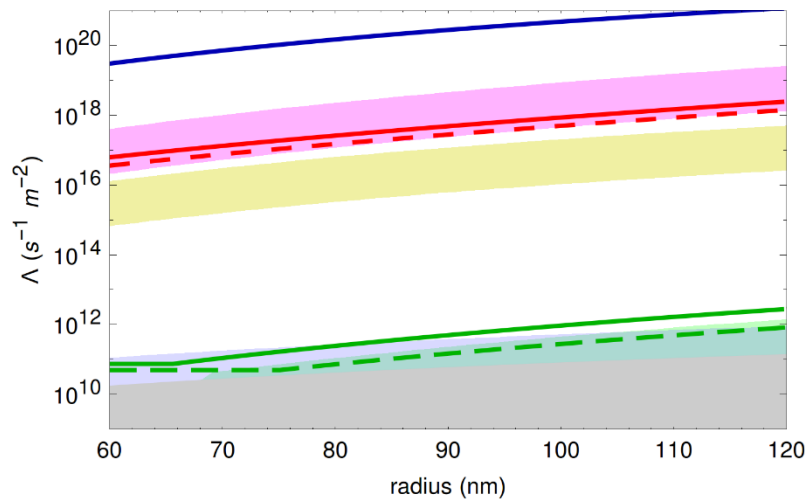


Figure 5: Comparison of theoretical predictions, sensitivity and sci. requirements. For the most part, this figure is the same as Figure 1. The only difference is the gray-shaded area, which represents a parameter range not accessible due to standard decoherence predicted by quantum theory given the scientific requirements given in Table 2. This illustrates that the scientific requirements allow to perform experiments over the full range of sensitivity of the MAQRO instrument.

## 4. Measurement concept

Here, we will describe the measurement concept we propose to fulfill the scientific requirements presented in section 3, and how to implement the measurements described and to achieve the science goals.

### 4.1. The optical bench

In order to achieve the scientific requirements on the initial quantum state for the experiments on wave-packet expansion and on high-mass matter-wave interferometry, we propose to use a cavity-optomechanical setup using optically trapped particles. It is paramount to use trapped particles instead of suspended mechanical oscillators because any mechanical suspension would potentially introduce decoherence due to phonon scattering, and it would limit the free evolution of the prepared quantum states [46–48]. While a recent ground-based proposal suggested using feed-back cooling of the 3D motion of a trapped particle to prepare particles for high-mass matter-wave interferometry [17], a cavity has the advantage of allowing effective cooling while still maintaining a macroscopic distance between the trapped particle and the rest of the optical setup. As we will be discussed below, this is paramount in the context of achieving the scientific requirements on environment conditions via passive radiative cooling.

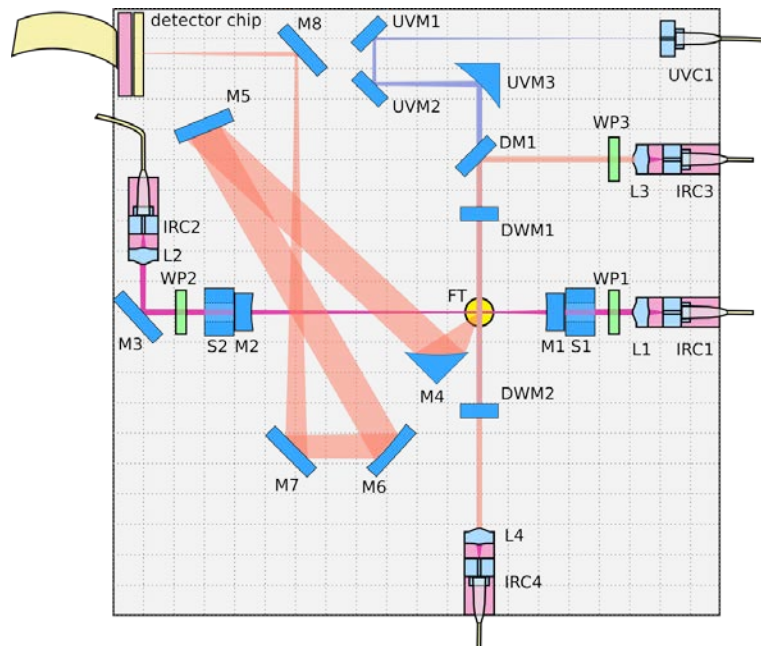


**Figure 6: Top view of the optical bench.** The optical bench is  $20 \times 20 \text{ cm}^2$  large. UVM: UV mirrors; M: IR mirrors; DM: dichroic mirrors; DWM: dual-wavelength mirrors; UVC: UV couplers; IRC: IR couplers; WP: quarter-wave plates; L: lenses; FT: base-plate feed-through S: spacers holding cavity mirrors. The mirrors M1 and M2 form a high-finesse IR cavity containing several modes (violet beam path originating at IRC1). DWM1 and DWM2 form a low-finesse cavity for IR light. The IR beam is indicated in light red, originating from IRC3 and coupled in again at IRC4. The UV beam originates at UVC1. The red-shaded, broad path indicates scattered-light imaging.

To achieve the low occupation numbers of the initial quantum state, we will aim at implementing a combination of passive and active cooling methods using multiple optical modes in a high-finesse optical cavity. The proposed approach is based on a modification of Ref. [49]. We are currently preparing a manuscript for publication describing this novel

method [50]. It will allow achieving the required low occupation numbers by using only cavity modes: two  $TEM_{00}$  modes for trapping and cooling along the cavity axis as has recently been achieved experimentally [39,51], plus  $TEM_{01}$  and  $TEM_{10}$  higher-order modes to allow for non-linear feedback to passively and actively cool the particle motion perpendicular to the cavity axis [50]. The cavity length is chosen to be approximately 10 cm in order to guarantee a small solid angle with optical bench elements. This is paramount to achieve low temperatures of the “test volume” immediately surrounding the test particle via passive cooling. To still achieve reasonable optomechanical coupling and high intensity at the trapping position, the cavity is chosen to be asymmetric with the two cavity mirrors having radii of curvature of 75 mm and 30 mm. The cavity finesse should be on the order of  $10^5$  but not less than  $3 \times 10^4$  [20].

The high-finesse cavity used for preparing the initial quantum state is the center piece of the scientific instrument of MAQRO. For increased stability and for easier alignment, the high-finesse cavity mirrors are mounted on blocks of ULE material with a center hole (“spacers” S1 and S2). The other central elements are a loading mechanism to load neutral, dielectric test particles into the optical trap and a CMOS camera to detect light scattered off the test particle. We propose to use 1064 nm infra-red (IR) light for the cavity because of the technological heritage from the LISA Technology package [52]. This will be used to measure the position of the test particle – a central prerequisite for all experiments of MAQRO. Additional information about the position can be gained from the frequency shift in the resonances for the various optical cavity modes used. For the experiment on high-mass matter-wave interferometry, we also need a standing-wave grating of 200 nm light. This requires optics for deep ultra-violet (DUV) light and a DUV fiber coupler. DUV fibers are, by now, commercially available, e.g., from Laser Components. A light source for this wavelength should be realistic to implement in space based on frequency quintupling of 1064 nm light [53]. Figure 6 shows the proposed design of the optical bench hosting the cavity, the CMOS detector chip and various fiber couplers to supply the IR and DUV light. In addition, there are dual-wavelength mirrors DWM1 and DWM2. Both should be reflective for IR light to form a low-finesse cavity, DWM1 should transmit DUV light, DWM2 should reflect DUV light to form the standing-wave grating for high-mass matter-wave interference. The finesse of the IR cavity formed by DWM1 and DWM2 should be  $\lesssim 30$ . This limit is imposed by requiring that the laser stay locked to the cavity even during the free-fall times of 100 s when the cavity field is switched off [20]. IR and DUV light are combined using the dichroic mirror DM1. Light of these two wavelengths is supplied to the OB and coupled back from the OB via DUV couplers UVC1-2 and IR couplers IRC1-4. The region denoted as FT (feed-through) is a hole through the optical-bench base plate. It allows test particles to be passed from below the optical bench (see subsection 4.3) to the trapping region within the IR cavity. The four optical modes for the cavity are supplied via a few-mode fiber and coupled directly into the cavity after passing through a quarter-wave plate. This option for coupling is present at both ends of the cavity, which provides a back-up option and allows gaining information by analyzing light transmitted through the cavity.

## 4.2. Fulfilling the requirements on temperature and vacuum

To achieve the low environment temperature and residual gas pressure, we propose to adapt the approach suggested earlier in the context of MAQRO [19,20] and various papers [41,54]. In particular, we propose to place the optical bench outside of the spacecraft to be passively radiatively cooled while being thermally insulated via consecutive shields as illustrated in Figure 7.

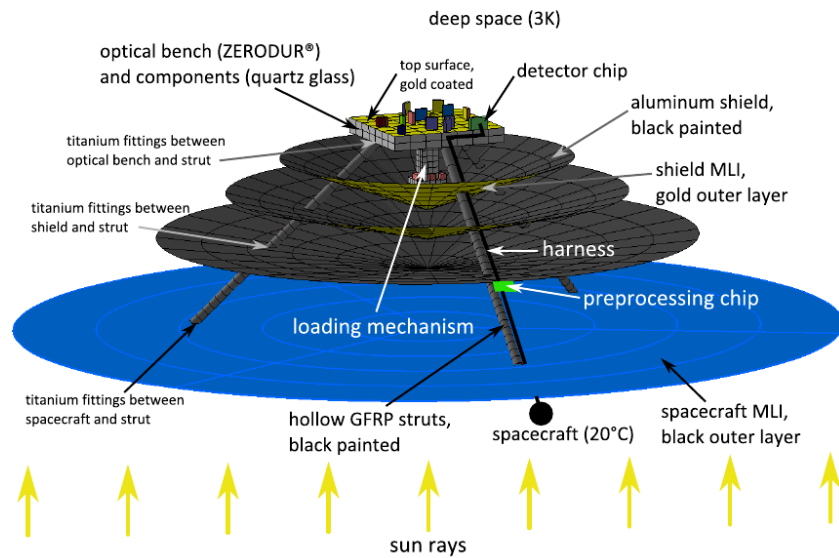


**Figure 7: CAD drawing of the geometric mathematical model of the MAQRO instrument.** The structure is attached outside the spacecraft, facing away from the sun. Three glass-fiber reinforced plastic (GFRP) struts hold three consecutive shields insulating the optical bench from the hot spacecraft surface (Image Source: Airbus Defence & Space, [41]).

Thermal studies using finite-element modelling showed [41,54] that this approach allows achieving temperatures as low as 25 K for the optical bench (OB) and  $\approx 11$  K for a small “test volume (TV)” around the position where the test particle is trapped. By increasing the size of the thermal shields such that it still fits into a Soyuz Fregat (2.8 m), one can reduce the OB temperature to 19 K, and the TV temperature to 10 K [41]. This latter option may be preferable to be on the safe side regarding the environment and particle temperatures.

For such low temperatures, we showed in earlier works [19] that outgassing of the components on the optical bench becomes negligible, and that the vacuum conditions on the OB will be determined by the vacuum in interplanetary space. Particles from hotter parts of the spacecraft or the thrusters will have high enough thermal energy to escape the gravitation of the spacecraft. Moreover, the spacecraft and the thermal shields will result in a wake effect further reducing the particle density expected. Given a particle density of  $500 \text{ cm}^{-3}$  for interplanetary space [55], we expect a density of  $\approx 50 \text{ cm}^{-3}$  in the experimental region above the OB. This is more than sufficient to fulfill the scientific requirements of MAQRO regarding the vacuum conditions.

In order to fulfill the temperature requirements of MAQRO, it is paramount to keep any optical or electrical dissipation at a minimum. With respect to the CMOS camera, MAQRO benefits from technological heritage from the James Webb Space Telescope (JWST). For that mission, a low-dissipation CMOS camera was developed [56]. The idea is to place a low-dissipation CMOS detector chip ( $\lesssim 1 \text{ mW}$ ) on the optical bench, to place the preprocessor electronics ( $\lesssim 10 \text{ mW}$ ) [56] in a warmer part of the shield structure, and to place the data procession inside the spacecraft. Still, the dissipation of the CMOS detector chip is one of the limiting factors in the passive-cooling approach of MAQRO. Slight improvements in the temperature of the OB could be achieved by further reducing this source of dissipation [41].

### 4.3. Loading test particles into the high-finesse cavity

We want to realize a reliable mechanism for loading dielectric test particles into the high-finesse cavity with as little dissipation as possible close to the optical bench. Moreover, the mechanism has to supply uncharged particles of sufficiently low temperature for tests using wave-function expansion (section 3.2) and high-mass matter-wave interferometry (section 3.3). For tests on the heating of the motion of trapped particles, the test particles should have a well-defined charge (section 3.1).

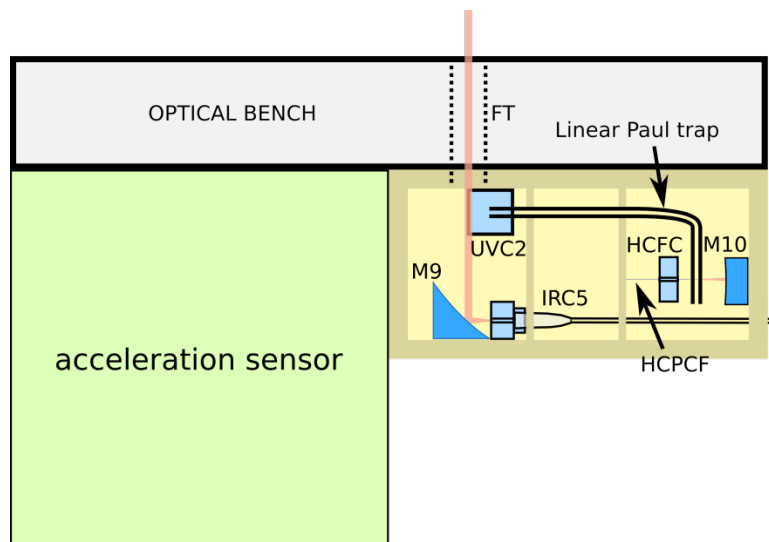


**Figure 8: Side view of the loading mechanism.** The image illustrates the three sub-divisions of the loading-mechanism chamber. The HCPCF is mounted on a fiber coupler (HCFC) close to the four rod-like electrodes of a linear Paul trap. At this position, the test particles are handed over from the guiding fiber to the Paul trap. This is also where the buffer gas will leave the chamber via the HCPCF. The particles are guided close to a UV coupler UVC2 where UV light is used to discharge them. Finally, they will enter an IR beam propelling the particles to the top of the optical bench.

To this end, we suggested [20] a mechanism consisting of two parts, one inside the spacecraft and one part directly below the OB. Inside the spacecraft, we propose that test particles are trapped optically in a sealed chamber filled with buffer gas (we propose Helium). The pressure inside this chamber can be high enough to allow optical trapping without a need for cooling the center-of-mass motion. The particles trapped should be charged negatively. They are then transferred into a hollow-core photonic-crystal fiber (HCPCF) and transferred along the fiber using an optical conveyor belt [57] in combination with a linear Paul trap using electrodes integrated in the fiber [58].

The HCPCF (incl. the electrodes) then guides the particles outside the spacecraft to a region below the OB containing the final stage of the loading mechanism (see Figure 8). Along the path of the HCPCF, the temperature of the buffer gas will drop, ideally to equilibrium with the environment temperature of the thermal shields and the OB. The temperature of the trapped particles will be cooled by the buffer gas.

Using charged particles during the transport from the spacecraft to the OB has the advantage that we do not need strong optical fields for guiding the particle, which would lead high particle temperatures. For the experiments on wave-packet expansion and matter-wave interferometry we will, however, need uncharged particles. This should be achievable by irradiating the

charged particles with DUV radiation [59] as we indicated in Figure 8.

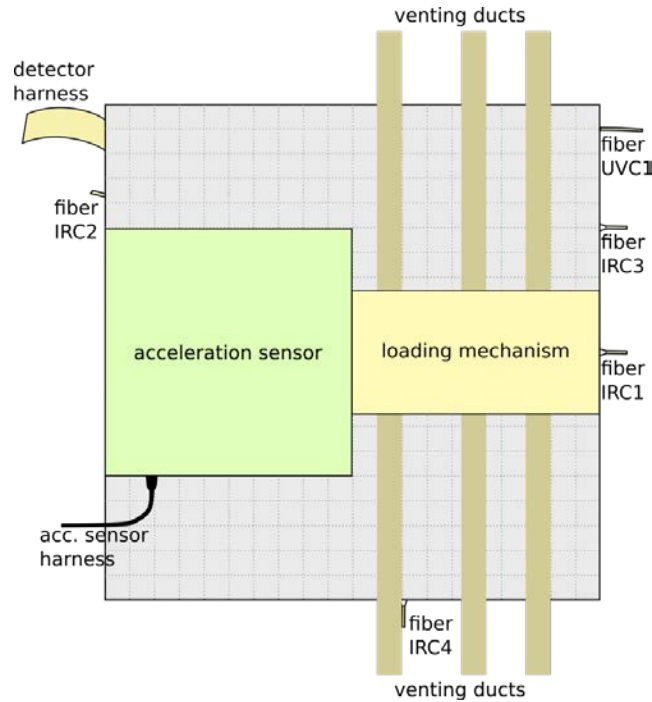


**Figure 9: Bottom view of the optical bench.** The image illustrates where venting ducts could be placed to minimize the amount of buffer gas potentially leaking to the experimental region. The figure also shows the position of the external acceleration sensor and fibers from the top of the optical bench.

In order to fulfill the stringent vacuum requirements of MAQRO despite the buffer gas, the loading mechanism below the optical bench is contained in a chamber divided into multiple sub-chambers. Each of these sub-chambers is designed to directly outgas to space (see Figure 8 and Figure 9). The overall concept of the loading mechanism is still in very early stages whereas parts of the mechanism have recently been demonstrated in the laboratory [57]. In terms of technology development, this surely is the most pressing issue. We will also discuss this issue in section 5.2.

#### 4.4. Laser system

As we indicated earlier, we plan to optically trap dielectric particles, and to cool their center-of-mass motion using multiple optical modes coupled to a high-finesse cavity. That means, we initially prepare four  $TEM_{00}$  modes and then combine them using spatial-mode division multiplexing. In Figure 10, we illustrate how we prepare the four modes originating from a single laser. The whole setup can be implemented using fiber components. Few-mode spatial-mode division multiplexers are available commercially (Modular Photonics).

Based on LISA Pathfinder [1,60], LISA [52,61] and the LISA Technology Package (LTP) [62], there exists strong technological heritage for optics, optical detection, optical fibers, acousto-optic modulation, electro-optic modulation and low-noise laser systems for 1064 nm. All optical (IR) technology required for MAQRO beyond that is available commercially but will still need some development to increase the TRL towards space-readiness.

While a space-ready, coherent source of light of about 200 nm is not readily available, this

should be achievable via comparatively simple modifications of an existing stable, all-solid-state technique [53] to adapt it from frequency quintupling of 1565nm to frequency quintupling of 1064nm. What is the power we need? We mentioned earlier, that the power needs to be higher for smaller particles. For a duration of 1μs of the grating and a fused-silica particle of mass  $m = 10^8$  amu, the optical power would need to be 5 mW, for a mass of  $m = 10^9$  amu, the required power would still be 0.5 mW. For  $m = 10^8$  amu, we can instead use a phase grating with  $\lambda_G = 1064$  nm. For that wavelength, the necessary power of 6mW is easy to supply – in particular, if we use a low-finesse IR cavity for enhancing the power applied.

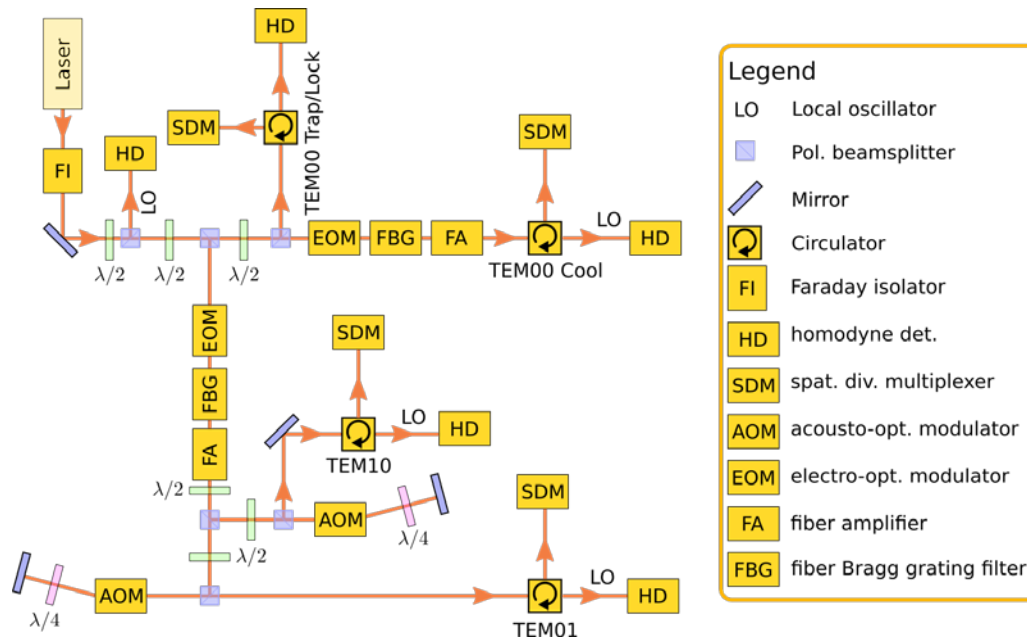


**Figure 10: Preparation of modes and optical detection.** We first prepare four modes and combine them in a spatial-mode division multiplexer (SDM). Its output supplies MAQRO’s optical bench. Optical signals returning the same way can be isolated using fiber circulators. They are then overlapped with the corresponding local oscillators (Los) to perform homodyne detection (HD). We use narrow-band fiber-Bragg gratings (FBGs) to filter sidebands generated using electro-optic modulators. Acousto-optic modulators are used to shift the frequencies of two modes. Fiber amplifiers (FAs) are used to amplify filtered sidebands where necessary.

## 4.5. Inertial sensors

The long free-fall times required (100 s) put strict requirements on the microgravity environment of MAQRO. That spacecraft and test particle experience slightly different gravitational fields can result in inaccurate measurements of the particle position. If we are to compensate for the gravitational field of the spacecraft or if we want to compensate solar radiation pressure acting on the spacecraft, we have to use micro thrusters. However, such thrusters inevitably have force-noise, which effectively leads to a random walk of the spacecraft. If this random walk is known, then changes of the position of the spacecraft relative to the test particle can be taken into account in the measurement results. If the random walk is not known, then it may blur interference patterns similar to decoherence. In particular, if we assume white thruster force noise  $FN_0$  ( $N/\sqrt{Hz}$ ), then the effect of thruster noise on the interference pattern can be described via an effective “decoherence” parameter:

$$\Lambda_{th} = \frac{2 FN_0^2 m^2}{\hbar^2 M^2}. \quad (9)$$

Here,  $M$  is the mass of the spacecraft, and  $m$  is the mass of the test particle. As an example, for

$M = 250 \text{ kg}$ ,  $m = 10^{10} \text{ amu}$ , and for a thruster force noise of  $FN_0 = 100 \text{ nN}/\sqrt{\text{Hz}}$  as in LPF, we get  $\Lambda_{\text{th}} = 8 \times 10^{15} \text{ m}^{-2} \text{ s}^{-1}$ . This shows that thruster noise is a critical issue. As mentioned earlier, this is not a problem if the random walk of the spacecraft is known to high enough precision. The required precision is not the same for all three spatial directions.

Parallel to the UV beam, the effective “decoherence” due to the random walk has to fulfill  $\Lambda \gtrsim \Lambda_{\text{min}}$ . In terms of accuracy for acceleration measurements this corresponds to  $\lesssim 1 \text{ (pm/s}^2\text{)}/\sqrt{\text{Hz}}$ . Parallel to the high-finesse cavity, we need an accuracy of 500nm for accurately measuring wave-function expansion (see section 3.2). This results in  $\lesssim 500 \text{ (pm/s}^2\text{)}/\sqrt{\text{Hz}}$  accuracy for acceleration measurements. Perpendicular to the OB, the requirement is more relaxed because the position only has to be known better than the waist of the high-finesse cavity mode ( $\sim 60\mu\text{m}$ ). This results in  $\lesssim 5 \text{ (nm/s}^2\text{)}/\sqrt{\text{Hz}}$  for acceleration measurements. To achieve this accuracy, we propose using two capacitive inertial sensors. One close to the test particle, the other one inside the spacecraft. Also, the high accuracy needed parallel to the UV grating can best be achieved by taking advantage of the cryogenic temperatures at the OB for the inertial sensor [63]. The advantage of this sensor is also that it can be separated in the sensor core and the sensor electronics. The former as low dissipation (0.1 mW) and can be placed close to the OB. The latter can be placed inside the spacecraft.

## 4.6. Orbit requirements

Due to MAQRO’s requirements on the environment temperature, the vacuum conditions as well as on the microgravity environment, the ideal orbit would be around the sun/earth Lagrange point L2. L1 would also be possible but has the disadvantage that several mW of thermal radiation from Earth would reach MAQRO’s optical bench. For an orbit around L1, we would follow LISA Pathfinder’s example: the MAQRO space-craft would be injected into a halo orbit around the sun/earth Lagrange point L1 (L2 would be a feasible alternative), following the initial injection into elliptical earth orbit and 8 apogee raising orbits. For an orbit around L2, similar considerations are applicable.

A highly elliptical orbit (HEO) could be a potential alternative. Due to the passive cooling approach of MAQRO, the distance of the apogee from Earth would have to be comparable with the distance to the Lagrange points L1/L2 in order to allow sufficient time for passive cooling and outgassing plus sufficient time for measurements. The advantage would, of course, be that such an orbit could allow combinations with instruments that need large gravity gradients like, e.g., STE-Quest.

Another feasible alternative to an L1/L2 orbit would be the orbit suggested for ASTROD I, although it would have to be investigated in more detail how the necessary pointing of the optical telescope of ASTROD I would influence the performance of MAQRO.

## 4.7. Technical Requirements

Table 3 provides an overview of the technical requirements of MAQRO.

Parameter	Requirement
Nominal mission lifetime (without possible extension)	2 years
Environment temperature	< 20K
Acceleration sensitivity	
along UV cavity	$\lesssim 1 \text{ (pm/s}^2\text{)}/\sqrt{\text{Hz}}$
along IR cavity	$\lesssim 500 \text{ (pm/s}^2\text{)}/\sqrt{\text{Hz}}$
perpendicular to optical bench	$\lesssim 5 \text{ (nm/s}^2\text{)}/\sqrt{\text{Hz}}$
Optical-trapping occupation number	
along cavity	$\sim 10$
orthogonal to cavity	$\sim 10^4$
Period of phase grating	100nm
Accuracy of position detection	
along UV cavity	$\ll 100\text{nm}$
along IR cavity	$\lesssim 500\text{nm}$
perpendicular to optical bench	$\ll 60\mu\text{m}$
Time for on-demand particle loading	$\ll 100\text{s}$
Measurement time per data point	$\lesssim 100\text{s}$
Vacuum – particle density	$< 500 \text{ cm}^{-3}$
IR-cavity finesse	$\gtrsim 3 \times 10^4$
Finesse of low-finesse IR cavity	$\lesssim 30$

Table 3: Overview of the technical requirements of MAQRO. See also Table 1 and Table 2.

## 5. Technology development

Here, we will discuss technology that needs further development, several critical issues that have to be solved, and we will present a rough draft of a roadmap of technology development.

### 5.1. Technical issues

Some of the key technologies of MAQRO already exist either in the lab or are even available commercially. Nevertheless, they will need further development to achieve space readiness. In Table 4, we provide an overview of such technologies and their current development status.

Parameter	Status	TRL
Spatial-mode division multiplexing	Integrated optics, commercially available, needs customization and testing	3
Coherent source deep-UV	Readily achievable in the lab	3
CMOS technology for < 20 K	Heritage from JWST for < 30 K	3-5
Adhesive or hydroxyl catalysis bonding of high-finesse cavities	Demonstrated at room temperature	3
Narrow-band filtering using Fiber-Bragg gratings	Commercially available	3
GHz spectrum analyzer	Commercially available	3
GHz function generator	Commercially available	
Passive radiative cooling approach	Concept demonstrated in multiple missions. Precise layout feasibility shown	2-5



	in multiple detailed studies	
Preparation of optically trapped particles close to quantum ground state	Feasibility shown in multiple experiments.	3
Optomechanical preparation using only cavity modes	Theoretical concept developed and feasibility shown	2-3
Optical conveyor belt for dielectric particles inside hollow-core fibers	Experimentally demonstrated	3
DUV fibers	Commercially available	3
Single-mode, polarization maintaining fiber	Commercially available	3

Table 4: Overview of technologies that need further development.

## 5.2. Critical issues

While the previous subsection described technologies that are already relatively mature, here we will discuss any issues where it is potentially unclear whether the suggested approaches will succeed. Actually, these are all related issues because they all concern the mechanism to load particles into the optical cavity.

### Issue 1: Buffer-gas cooling inside the hollow-core fibers

- Will the transported particles cool sufficiently quickly?
- How will the buffer-gas affect the vacuum level on the optical bench?
- Will we have to realize a valve to stop buffer-gas from leaking continuously?
- While several papers have demonstrated the feasibility of including electrodes in hollow-core fibers [58], using them as linear Paul traps for charged, dielectric particles yet has to be demonstrated.

### Issue 2: Discharging of the test particles

- Can we completely discharge the particles? Experiments in the Geraci group showed a reduction of charges, but zero charge has not been attained so far [59,64].
- How long will the discharging take? The particle loading (including discharging) should take significantly less time than the time of a measurement run. In [64], the discharging down to a few charges took up to two minutes.

### Issue 3: Particle temperature

- If the buffer-gas approach works, the particle temperature should fulfill the requirements until it is loaded into the optical trap. Then it will be important to do the optical manipulation as quickly as possible to not heat the particle. This time should stay on the millisecond level.
- We assumed the particles to have similar optical properties as the bulk materials. Depending on the method of particle fabrication, the particles can, however, be severely contaminated. This would lead to excessive heating in the optical trap. Using very clean particles will, therefore, be a critical aspect of MAQRO.

### 5.3. Technology roadmap

It should be possible to cover the technical issues listed in Table 4 of subsection 5.1 relatively quickly within a few years of time, depending on how many groups will be involved. There are no potential showstoppers among those technologies.

More effort will be necessary to address the critical issues presented in subsection 5.2. In this context, it will be important that several groups in the consortium perform a concerted effort to test specific aspects of the technologies required.

In particular, it will be important to study the precise requirements the loading mechanism as well as the optical trap have to fulfill in order to achieve low enough particle temperatures. Moreover, the combination of loading in a buffer-gas chamber, the transport into a vacuum environment and the discharging of the particle will have to be studied in detail.

## 6. Other information

The “Scientific Idea” of MAQRO has met rapidly increasing interest from groups in several member states of ESA but also from groups in the US. Of course, a collaboration with American partners would be interesting in the future. Currently, three groups in the US support the idea of MAQRO. Within Europe, there already exists interest in Austria, France, Germany, Hungary, Italy, Switzerland, and the UK. Moreover, there exists potential interest in the Czech Republic, the Netherlands, Spain, and Portugal. Apart from these countries, there are existing and potential partners in Australia.

In the course of the present Call for New Science Ideas by ESA, other new ideas are submitted as proposals. In particular, these concern the potential use of optomechanical sensors for dark matter as well as additional tests of quantum physics versus alternative “Schrödinger-Newton”-type models. MAQRO could potentially also provide an interesting platform for these experiments. This would have to be investigated more closely in the study phase.



## A. Abbreviations

<b>Abbreviation</b>	<b>Description</b>
AOM	acousto-optic modulator
AMU	atomic mass unit
AU	astronomical unit
BBO	beta-Barium Borite
CMOS	Complementary metal-oxide semi-conductor
CSL	Continous spontaneous localization
DFACS	drag-free attitude and control system
DP model	Diósi-Penrose model
DUV	Deep ultra-violet
EOM	electro-optic modulator
HEO	Highly-elliptical orbit
IR	Infrared
JWST	James Webb Space Telescope
HCPCF	hollow-core photonic-crystal fiber
K model	Károlyházy model
L1/L2	Lagrange points L1/L2 of Sun/Earth system
LEO	Low Earth orbit
LISA	Laser Interferometer Space Antenna
LM	loading mechanism
LPF	LISA Pathfinder
LTP	LISA Technology Package
MAQRO	Macroscopic Quantum Resonators
PDH	Pound-Drever-Hall
QG model	Quantum-gravity model of Ellis et al.
QM	quantum mechanics
S/C	spacecraft
SC	spacecraft
SHG	second-harmonic generation
SiC	Silicon Carbide
TRL	Technology readiness level
UHV	ultra-high vacuum
ULE	ultra-low expansion
UV	Ultra-violet
VIS	visible light

## B. Bibliography

- [1] M. Armano et al., Phys. Rev. Lett. **116**, 231101 (2016).
- [2] B. P. Abbott et al., Phys. Rev. Lett. **116**, 61102 (2016).
- [3] V. B. Braginsky, A. B. Manukin, and M. Y. Tikhonov, Sov. Phys. JETP **31**, 829 (1970).
- [4] C. M. Caves, K. S. Thorne, R. W. P. Drever, V. D. Sandberg, and M. Zimmermann, Rev. Mod. Phys. **52**, 341 (1980).
- [5] A. D. O’Connell et al., Nature **464**, 697 (2010).
- [6] J. D. Teufel et al., Nature **475**, 13 (2011).
- [7] J. Chan et al., Nature **478**, 89 (2011).
- [8] A. Bassi and G. C. Ghirardi, Phys. Rep. **379**, 257 (2003).
- [9] A. Bassi, E. Ippoliti, and S. Adler, Phys. Rev. Lett. **94**, 30401 (2005).
- [10] A. Bassi, K. Lochan, S. Satin, T. Singh, and H. Ulbricht, Rev. Mod. Phys. **85**, 471 (2013).
- [11] E. Schrödinger, Naturwissenschaften **23**, 807 (1935).
- [12] C. Davisson and L. H. Germer, Nature **119**, 558 (1927).
- [13] G. P. Thomson, Nature **120**, 802 (1927).
- [14] I. Estermann and O. Stern, Z. Phys. **61**, 95 (1930).
- [15] S. Eibenberger, S. Gerlich, M. Arndt, M. Mayor, and J. Tüxen, Phys. Chem. Chem. Phys. **15**, 14696 (2013).
- [16] S. L. Adler and A. Bassi, Science **325**, 275 (2009).
- [17] J. Bateman, S. Nimmrichter, K. Hornberger, and H. Ulbricht, Nat. Commun. **5**, 4788 (2014).
- [18] H. Pino, J. Prat-Camps, K. Sinha, B. P. Venkatesh, and O. Romero-Isart, 20 (2016).
- [19] R. Kaltenbaek et al., Exp. Astron. **34**, 123 (2012).
- [20] R. Kaltenbaek et al., EPJ Quantum Technol. **3**, 5 (2016).
- [21] M. Aspelmeyer, T. J. Kippenberg, and F. Marquardt, Rev. Mod. Phys. **86**, 1391 (2014).
- [22] H. Miao, Y. Ma, C. Zhao, and Y. Chen, Phys. Rev. Lett. **115**, 211104 (2015).
- [23] E. Oelker et al., Phys. Rev. Lett. **116**, 41102 (2016).
- [24] D. Goldwater, M. Paternostro, and P. F. Barker, Phys. Rev. A **94**, 10104 (2016).
- [25] B. Collett and P. Pearle, Found. Phys. **33**, 1495 (2003).
- [26] R. Kaltenbaek and M. Aspelmeyer, in *Erwin Schrödinger - 50 Years After*, edited by W. L. Reiter and J. Yngvason (2013), pp. 123–132.
- [27] S. Bera, B. Motwani, T. P. Singh, and H. Ulbricht, Sci. Rep. **5**, 7664 (2015).
- [28] M. A. Schlosshauer, *Decoherence and the Quantum-to-Classical Transition* (Springer,

- Berlin, 2007).
- [29] G. C. Ghirardi, A. Rimini, and T. Weber, *Phys. Rev. D* **34**, 470 (1986).
  - [30] P. Pearle, *Phys. Rev. A* **39**, 2277 (1989).
  - [31] G. C. Ghirardi, P. Pearle, and A. Rimini, *Phys. Rev. A* **42**, 78 (1990).
  - [32] N. Gisin, *Helv. Phys. Acta* **62**, 363 (1989).
  - [33] S. L. Adler, *J. Phys. A Math. Theor.* **40**, 2935 (2007).
  - [34] J. Ellis, S. Mohanty, and D. V Nanopoulos, *Phys. Lett. B* **221**, 113 (1989).
  - [35] L. Diósi, *J. Phys. A Math. Theor.* **40**, 2989 (2007).
  - [36] R. Penrose, *Gen. Rel. Grav.* **28**, 581 (1996).
  - [37] F. Karolyhazy, *Nuovo Cim. A* **42**, 390 (1966).
  - [38] M. Bahrami, M. Paternostro, A. Bassi, and H. Ulbricht, *Phys. Rev. Lett.* **112**, 210404 (2014).
  - [39] J. Millen, P. Z. G. Fonseca, T. Mavrogordatos, T. S. Monteiro, and P. F. Barker, *Phys. Rev. Lett.* **114**, 123602 (2015).
  - [40] T. H. Kim, P. F. Herskind, T. Kim, J. Kim, and I. L. Chuang, *Phys. Rev. A* **82**, 43412 (2010).
  - [41] A. Pilan Zanoni et al., *Appl. Therm. Eng.* **107**, 689 (2016).
  - [42] G. D’Ariano and H. Yuen, *Phys. Rev. Lett.* **76**, 2832 (1996).
  - [43] O. Romero-Isart, *Phys. Rev. A* **84**, (2011).
  - [44] K. Hornberger, S. Gerlich, P. Haslinger, S. Nimmrichter, and M. Arndt, *Rev. Mod. Phys.* **84**, 157 (2012).
  - [45] B. Brezger, M. Arndt, and A. Zeilinger, *J. Opt. B Quantum Semiclassical Opt.* **5**, S82 (2003).
  - [46] D. E. Chang et al., *Proc. Natl. Acad. Sci. U. S. A.* **107**, 1005 (2010).
  - [47] O. Romero-Isart, M. L. Juan, R. Quidant, and J. I. Cirac, *New J. Phys.* **12**, 33015 (2010).
  - [48] P. F. Barker and M. N. Shneider, *Phys. Rev. A* **81**, 23826 (2010).
  - [49] Z. Yin, T. Li, and M. Feng, *Phys. Rev. A* **83**, 13816 (2011).
  - [50] M. Bathaee and others, *Active and Passive Three-Dimensional Cavity-Selfcooling of Nanoparticles* (2016).
  - [51] N. Kiesel et al., *Proc. Natl. Acad. Sci. U. S. A.* **110**, 14180 (2013).
  - [52] M. Tröbs et al., *Class. Quantum Gravity* **23**, S151 (2006).
  - [53] S. Vasilyev et al., *Appl. Phys. B* **103**, 27 (2011).
  - [54] G. Hechenblaikner et al., *New J. Phys.* **16**, 13058 (2014).
  - [55] L. Biermann, *Obs.* **77**, 109 (1957).

- [56] M. Loose, J. Beletic, J. Garnett, and N. Muradian, in *SPIE Astron. Telesc. + Instrum.*, edited by J. C. Mather, H. A. MacEwen, and M. W. M. de Graauw (International Society for Optics and Photonics, 2006), p. 62652J–62652J–11.
- [57] D. Grass, J. Fesel, S. G. Hofer, N. Kiesel, and M. Aspelmeyer, *Appl. Phys. Lett.* **108**, 221103 (2016).
- [58] G. Chesini et al., *Opt. Express* **17**, 1660 (2009).
- [59] G. Ranjit, M. Cunningham, K. Casey, and A. A. Geraci, *Phys. Rev. A* **93**, 53801 (2016).
- [60] M. Armano et al., *Class. Quantum Gravity* **26**, 94001 (2010).
- [61] O. Jennrich, *Class. Quantum Gravity* **26**, 153001 (2009).
- [62] S. Anza et al., *Class. Quantum Gravity* **22**, S125 (2005).
- [63] L. Lafargue, M. Rodrigues, and P. Touboul, *Rev. Sci. Instrum.* **73**, 196 (2002).
- [64] J. H. Stutz, *Calibration of an Optically Levitated Microsphere as a Force Sensor*, University of Nevada, 2014.